

Investigation of NO Adsorption and Desorption Phenomena on a Pd/ZSM-5 Passive NO_x Adsorber

Yuntao Gu ^{a,‡}, Sreshtha Sinha Majumdar ^{b,‡}, Josh A. Pihl ^{b,*}, William S. Epling ^a

^a Department of Chemical Engineering,
University of Virginia, Charlottesville, VA 22903

^b Applied Catalysis and Emissions Research Group, National Transportation Research Center,
Oak Ridge National Laboratory, Oak Ridge, TN 37830

* Corresponding author; pihlja@ornl.gov,

‡ These authors contributed equally

This manuscript has been authored by UT-Battelle, LLC, under contract DE-AC05-00OR22725 with the US Department of Energy (DOE). The US government retains and the publisher, by accepting the article for publication, acknowledges that the US government retains a nonexclusive, paid-up, irrevocable, worldwide license to publish or reproduce the published form of this manuscript, or allow others to do so, for US government purposes. DOE will provide public access to these results of federally sponsored research in accordance with the DOE Public Access Plan (<http://energy.gov/downloads/doe-public-access-plan>).

Abstract

Pd-based zeolite materials have gained significant attention as passive NO_x adsorbers (PNAs) for diesel-engine cold-start NO_x mitigation due to their ability to store NO_x at low temperatures. Pd/ZSM-5 is a promising PNA candidate, however, the NO adsorption mechanism over this material is not well understood. This study combines flow reactor experiments and surface spectroscopy to investigate NO adsorption under a variety of conditions. The state of hydration of the Pd cations played an important role in determining the impact of H₂O and CO concentration on the PNA performance. Below 150 °C, the inhibition effect of H₂O on NO adsorption was mitigated by CO. Due to dehydration, neither H₂O nor CO had an impact on NO uptake at 150 °C, where maximum NO storage capacity of the PNA was also observed. The observed gas composition and temperature effects on NO adsorption and formation of surface intermediates ultimately inform a proposed mechanism.

Key words: Cold start; Emissions; Passive NO_x adsorber; NO_x storage; Adsorption mechanism; Palladium zeolite catalyst

1. Introduction

NO_x (oxides of nitrogen) abatement technologies for diesel-engine exhaust aftertreatment include state-of-the-art ammonia/urea selective catalytic reduction (SCR) systems which are effective above 200 °C [1–3]. Control of cold-start NO_x emissions below 200 °C is critical for meeting the increasingly stringent NO_x emissions regulations for lean-burn diesel-fueled vehicles, establishing a need for efficient low temperature catalysis and trap materials [4–8].

Multiple studies have investigated passive NO_x adsorbers (PNA), which trap NO_x at low temperatures and release NO_x at temperatures above which the urea SCR system can efficiently eliminate NO_x emissions from the vehicle [5,6,8–15]. Chen and coworkers were the first to report that Pd ion-exchanged zeolites show superior NO_x storage capacity and sulfur tolerance when compared to metal-oxide supported NO_x adsorbers under complex exhaust compositions [16]. Pd ion-exchanged zeolites have since garnered significant attention and studies are converging on the agreement that Pd²⁺ cations within the zeolite framework trap NO_x at low temperatures in the presence of excess oxygen typical of diesel-engine exhausts, thus providing a possible pathway to mitigating cold-start NO_x emissions [17–19]. The NO_x storage capacity, NO_x release temperature from the PNA, rate of NO_x adsorption and durability of the PNA have been found to be influenced by several parameters such as the type of zeolite, synthesis method, activation strategy, and exhaust composition [6,9,14,17,20–24].

Pd/BEA, Pd/SSZ-13 and Pd/ZSM-5 exhibit significant NO_x trapping capacities; however, their NO_x desorption profiles, specifically the temperature window of NO_x release, appear unique to the type of PNA [12,16]. The relatively low NO_x desorption temperature window for Pd/BEA (180 - 250 °C) could result in NO_x release before the downstream SCR catalyst can achieve high NO_x conversions while the higher NO_x desorption temperature for Pd/SSZ-13 (280 - 450 °C) could make regeneration of the PNA challenging under realistic exhaust conditions [12,14,16,25]. For diesel engine aftertreatment systems, Pd/ZSM-5 is promising as a PNA since its NO_x release temperature window is between 200 to 400 °C [11,12,16]. Furthermore, Pd/ZSM-5 has also been reported to simultaneously trap hydrocarbon species along with NO at low temperatures, making it potentially a bi-functional trapping material for cold-start applications [26].

Pd speciation and the NO adsorption mechanism on Pd/zeolites have been extensively investigated under idealized conditions [27–30]; however, while Pd/ZSM-5 is an interesting PNA candidate, the nature of Pd within a ZSM-5 zeolite and its speciation under realistic exhaust conditions is not well understood, which is critical to fully understand the NO adsorption mechanism. While experimental studies on PNAs have proposed several possible NO_x storage sites and NO_x adsorption mechanisms, the literature has not converged on the mechanism of a system that involves H₂O, NO and CO [12,22,31–33].

The current contribution focuses on gaining a better understanding of the underlying chemistry involved in the NO adsorption and desorption phenomena on Pd/ZSM-5 PNAs through flow reactor experiments and in-situ diffuse reflectance infra-red Fourier-transform spectroscopy (DRIFTS) investigations. The flow reactor experiments include a systematic study on the effects of gas composition (including changes in NO, CO, O₂, H₂O and CO₂ concentrations) and

temperature on PNA NO uptake and release. DRIFTS studies were used to characterize surface species formed during NO adsorption and the effect of hydration, NO adsorption temperature, and CO on Pd speciation. A mechanism capturing the key observations from the flow reactor experiments and the surface intermediates confirmed by DRIFTS studies is proposed, which could form the foundation for future modelling efforts as well as inform future PNA formulation efforts.

2. Experimental Methods

2.1. Passive NO_x adsorber (PNA)

The core sample (2.0 cm by 5.0 cm) used in this study is a model Diesel Cold Start Catalyst Concept (dCSC™) component obtained from Johnson Matthey. The passive NO_x adsorber (PNA) was Pd-exchanged ZSM-5 with a Pd loading of 1.8g/L. The PNA was washcoated onto a 400 cpsi cordierite monolith core. The PNA was degreened at 600 °C for 4 h in 10% O₂ and 7% H₂O prior to running any experiments.

2.2. Set-up for flow reactor experiments

A LabVIEW (National Instruments)-controlled synthetic exhaust flow reactor system was used to conduct NO uptake/release experiments on the PNA. The reactor schematic is shown elsewhere [34,35]. MKS Instruments mass-flow controllers were used to vary the composition of the feed to understand the impact of the various constituents on NO adsorption on the PNA. Water vapor was added into the reaction mixture using an HPLC pump (Eldex Optos 1LMP) and a custom-built water-preheater assembly [34]. Pneumatically controlled 4-way valves (Valco A24UWE) were used to introduce CO and NO to achieve step changes in composition during the bypass and adsorption steps.

The Pd/ZSM-5 core sample was wrapped in non-woven alumina (Cotronics) tape and loaded in a 25 mm OD quartz tube. The quartz reactor tube was packed with smaller quartz tubes (3 mm OD, 1mm ID) upstream of the PNA core sample to increase heat transfer to the feed gas. To ensure isothermal conditions across the PNA, five K-type thermocouples were placed into the reactor at the following points: (i) 5 mm upstream of the catalyst inlet, (ii) in a central catalyst channel at the axial mid-point, (iii) in a radial catalyst channel at the axial mid-point, (iv) in a central catalyst channel at the catalyst outlet, and (v) in a radial catalyst channel at the catalyst outlet. The quartz tube reactor assembly was then placed into a furnace (Lindberg Blue/M), which was downstream from another identical furnace used to preheat the gases, to facilitate isothermal conditions. The exit stream composition from the reactor was analyzed using a Multigas 2030HS FTIR spectrometer (MKS Instruments). O₂ concentrations were not directly measured during these experiments. Inlet O₂ concentrations were verified from the flows measured by the mass flow controllers.

2.3. Experimental protocol: NO adsorption and temperature programmed desorption (TPD)

A systematic study was conducted by varying the NO exposure conditions (as summarized in Table 1 below) to understand the impact of each of the parameters on NO uptake and release.

Table 1: NO exposure conditions

Parameter	Range	Baseline Conditions
NO	25 - 1600 ppm	200 ppm
CO	50 - 800 ppm	200 ppm
O₂	1 - 13%	10%
H₂O	5 - 13%	7%
CO₂	0 - 13%	0%
N₂	--	Balance
Adsorption Temperature	75 - 225 °C	100 °C
Gas Hourly Space Velocity (GHSV)	--	30000 hr ⁻¹

The experimental protocol used to measure NO uptake and release is shown in Table 2; the temperatures and concentrations listed from step 3 to step 6 are for the “baseline” conditions, but they varied in other experiments. Concentrations for steps 1 and 2 are constant for all the experiments performed. Each experiment began with a pretreatment at 600 °C to ensure that all the NO stored in the prior experiment had been released and the Pd was in a fully oxidized state. After the pretreatment, the PNA sample was cooled to the desired operating temperature under the O₂, H₂O, and CO₂ concentrations used in the exposure step. After the PNA temperature was stable, CO was introduced. Five minutes later, NO was introduced. The NO exposure step continued until the measured NO outlet concentration achieved a steady state. The time to reach steady state varied with the NO concentration and temperature, but generally was 10-20 min. After the NO concentration achieved a steady state, the NO was switched off and the catalyst temperature was ramped to 600 °C at 20 °C/min. The catalyst was held at 600 °C for 10 min before proceeding to the next experiment.

Table 2. Experiment protocol with sample conditions

Step	Description	Time (min)	T (°C)	NO (ppm)	CO (ppm)	O₂ (%)	H₂O (%)
1	Pretreat	30	600	0	0	10	7
2	Cool	varies	600-100	0	0	10	7
3	Start CO	5	100	0	200	10	7
4	NO exposure	varies	100	200	200	10	7
5	TPD	25	100-600	0	200	10	7
6	Hold	10	600	0	200	10	7

2.4. In-situ diffuse reflectance infrared Fourier transform spectroscopy (DRIFTS)

In order to gain insights into the surface intermediates and reactions on the PNA during NO adsorption, experiments were conducted using DRIFTS on an Agilent Cary 670 FTIR spectrometer. A Harrick Praying Mantis DRIFTS accessory coupled with a liquid nitrogen-cooled mercury-cadmium-telluride (MCT) detector was used to collect the spectra. The DRIFTS accessory consisted of a Harrick high temperature reaction chamber with ZnSe windows along with gas flow capabilities designed for in-situ analysis of the surface of the sample. A thin layer of the washcoated sample ($\sim 0.3 \text{ cm}^2$) from the degreened Pd/ZSM-5 core was placed on a bed of stainless-steel beads in the sample holder. A bank of mass flow controllers was used to control the composition of the gas flowing over the sample. The NO, CO and O₂ concentrations matched those used in the flow reactor and are listed in Table 2. 1 or 4.5 % H₂O was introduced to the feed using a saturator immersed in a recirculating constant temperature bath. Prior to NO adsorption, the sample was pretreated at 550 °C in the presence of 10% O₂ for 30 min and then cooled to the relevant NO adsorption temperature in 10% O₂. 64 spectra were averaged for background collection under appropriate conditions and 32 spectra were averaged for sample spectra. Spectra were collected during NO adsorption under various feed conditions until saturation followed by temperature programmed desorption (TPD) from the adsorption temperature to 500 °C to release the stored NO. Additionally, the interaction between NO and CO during NO adsorption was investigated **by introducing CO before and during NO exposure.**

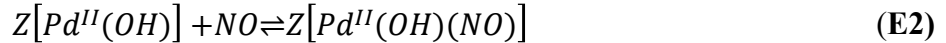
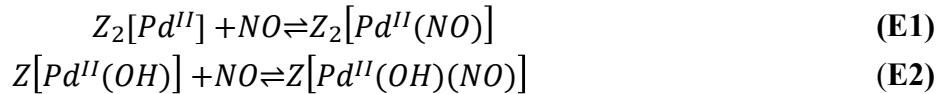
3. Results and Discussion

Consistent with previously reported observations, preliminary experiments revealed that the NO storage capacity of the Pd/ZSM-5 material initially decreased with each experiment [25,36,37]. Since this degradation confounded attempts to investigate the impacts of operating conditions on NO storage and release, dozens of NO storage-release cycles were conducted under the baseline conditions until the subsequent measured NO storage capacity was stable. The initial NO storage capacity corresponded to a NO:Pd ratio of 0.4 based on total Pd loading. After dozens of cycles, the stabilized NO:Pd ratio dropped to 0.2. While this Pd utilization is lower than what has been reported in the literature for other Pd-zeolite PNAs prior to any degradation, and is non-optimal from a device size and cost standpoint, experiments conducted still provide useful insights into the mechanisms for NO storage and release on the stable Pd sites still active for storage.

To characterize the initial Pd speciation in Pd/ZSM-5, in-situ DRIFTS spectra were collected during PNA exposure to 200 ppm NO and 10% O₂ under dry conditions, followed by an Ar purge. IR peaks at 2128 cm⁻¹, 1873 cm⁻¹, 1839 cm⁻¹ and the broad IR bands in the 1500 to 1700 cm⁻¹ range observed in **Figure 1** have been identified based on surface chemistry studies of the interaction between NO and Pd/ZSM-5 under ultra-high vacuum conditions [27,29,30,38,39]. The wide IR band centered at 2128 cm⁻¹ has been assigned to the linear N-O stretching frequency of NO⁺ interacting with AlO₂⁻ from the zeolite framework [30,38,40]. Consistent with observations reported in literature, the peak intensity at 2128 cm⁻¹ decreased significantly during the Ar purge

at 100 °C, indicating that this interaction is relatively weak [27]. **Formation of nitrates**, indicated by the IR bands in the 1600 cm⁻¹ region, can be facilitated via evolution of NO₂ by PdO and Bronsted acid sites [38,41]. However, the **nitrate species** are generally not coordinated with Pd cations and thus provide no information about the initial Pd speciation in the zeolite framework.

The IR peak assignments, 1873 and 1839 cm⁻¹, associated with NO adsorbed on cationic Pd species and the molecular structure of the corresponding surface intermediates are contentious in the literature. Descorme et al. assigned the two IR features at 1873 and 1839 cm⁻¹ to the stretching frequencies of NO directly coordinated with Pd²⁺ and Pd⁺ cations, respectively, and proposed the reduction of Pd²⁺ to Pd⁺ upon NO exposure, which was supported by simultaneous NO₂ formation [27]. The existence of Pd⁺ is where the contention lies, as direct characterization of Pd⁺ has only been reported for Pd/Y after H₂ exposure [42,43]. Pd²⁺ cationic species, on the other hand, have been more widely observed within different zeolitic systems, likely due to the thermodynamically favored four-coordinated structure [44]. Furthermore, the NO stretching frequencies of the Pd²⁺-NO complexes depend on the zeolite topology and aluminum distribution [18,28]. Although understanding the exact molecular structures of cationic Pd-NO species is not the focus of this work, **Figure 1** indicates that there are at least two different Pd-NO complexes in the absence of H₂O. We, therefore, attribute IR features at 1873 and 1839 cm⁻¹ to NO adsorbed on two different Pd²⁺ entities that locate at different ion-exchange positions, and experience different ligand environments, for example, Z₂Pd and ZPdOH. Hence, NO adsorption on cationic Pd under dry conditions can be represented by equations (E1) and (E2):



The proposed mechanism will be expanded from equations (E1) and (E2) in the following sections to incorporate the effects of changing the various NO exposure conditions summarized in Table 1 and to include the key surface intermediates identified through in-situ DRIFTS experiments.

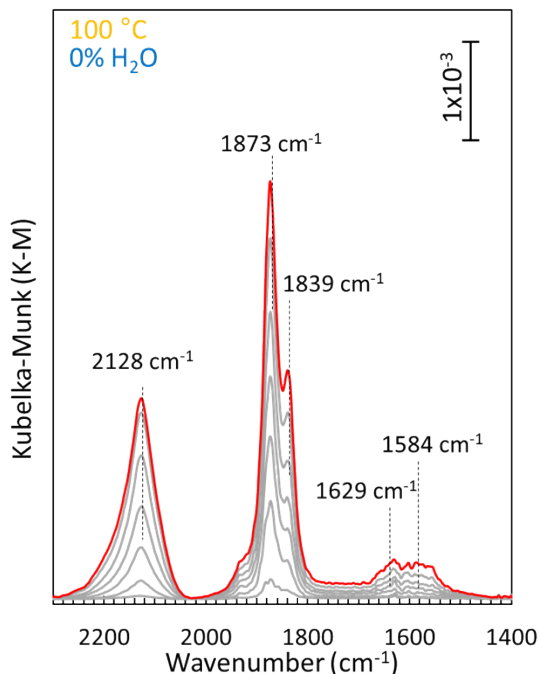


Figure 1: **In-situ** time-resolved DRIFTS spectra collected at 45 s intervals (final spectrum in red) during NO adsorption on a degreened Pd/ZSM-5 PNA sample at 100 °C under dry conditions. Feed conditions: 200 ppm NO, 10% O₂, balance N₂.

Once the stability of the PNA and initial Pd states were established, a systematic investigation was carried out by varying the NO exposure conditions to gain an understanding of the impact of each of the parameters in Table 1 on the NO storage and release. A separate set of experiments was conducted to understand the effect of each NO exposure parameter listed in Table 1. Every set of experiments included the baseline conditions to ensure consistency in the behavior of the PNA over time.

Figure 2 shows the measured catalyst temperatures and outlet concentrations of CO, NO, and CO₂ during an experiment conducted under the baseline NO exposure conditions detailed in Table 1. Aside from providing a visual summary of the protocol that was used for most of the experiments, this data set illustrates a few other key points about the behavior of the Pd/ZSM-5 PNA under the protocol used for this study. **Figure 2(a)** shows all five thermocouple temperatures and demonstrates that the PNA was under isothermal conditions (± 2 °C) during the adsorption step. The NO concentration profile in **Figure 2(b)** shows a delay between when the NO is first turned on and when NO is first observed in the reactor outlet, i.e., when NO starts to break through. This time period of complete uptake demonstrates that the Pd/ZSM-5 material is effective as a passive NO_x adsorber. Total NO uptake for each experiment was calculated by integrating the difference between the NO inlet concentration and the NO breakthrough profile. Total NO release was calculated by integrating the area under the NO concentration profile during the TPD. The calculated uptake and release were within experimental error for all the experiments conducted,

indicating that all the NO stored during the adsorption step is released during the TPD as NO; formation of other oxides of nitrogen such as NO₂ or N₂O was not observed during the experiments reported here.

In addition to providing a second measure of NO storage, the TPD portion of the experiment protocol also allows measurement of the temperatures at which NO is released from the Pd/ZSM-5 PNA. For the baseline experiment shown in **Figure 2** and all subsequent experiments below, the NO adsorbed on the PNA was released between 200 to 400 °C. Typical diesel exhaust systems rely on a urea selective catalytic reduction (SCR) system to eliminate NOx emissions from the vehicle when the exhaust temperature is above 200 °C. With NO release onset at 200 °C and NO being trapped at low temperatures, Pd/ZSM-5 has the right PNA properties to mitigate cold-start NOx emissions.

The CO concentration profile in **Figure 2(c)** shows two interesting features. At the very beginning of the experiment, when CO is first turned on, there is a period of time before the CO concentration reaches a steady state. Since the CO₂ concentration in **Figure 2(d)** is steady during the same time period, the slow approach of the CO concentration to steady state is likely due to CO being stored on the PNA. This explanation is further supported by the increase in CO concentration when NO is introduced – the NO appears to displace the CO from the storage sites. Integrating the transient CO profiles reveals that all the CO stored at the beginning of the experiment is released upon introduction of NO. This implies that NO adsorption strongly inhibits CO adsorption and there is no evidence for co-adsorption of NO and CO on this Pd/ZSM-5 under these operating conditions.

The CO₂ concentration profile in **Figure 2(d)** also yields some insights into the PNA behavior. CO₂ formation upon introduction of CO indicates activity for CO oxidation both catalytically and stoichiometrically even at 100 °C, the ratio between the two is better displayed in the supporting information **Figure S2**. This CO₂ formation almost completely disappears upon introduction of NO, consistent with the theory that the NO is displacing CO from the PNA as shown above and blocking the active sites for CO oxidation [40]. Additionally, a non-typical CO oxidation light-off behavior was observed during the temperature ramp at around 150 °C. As we will discuss later, this non-typical change in CO oxidation activity is due to the dehydration of Pd cations.

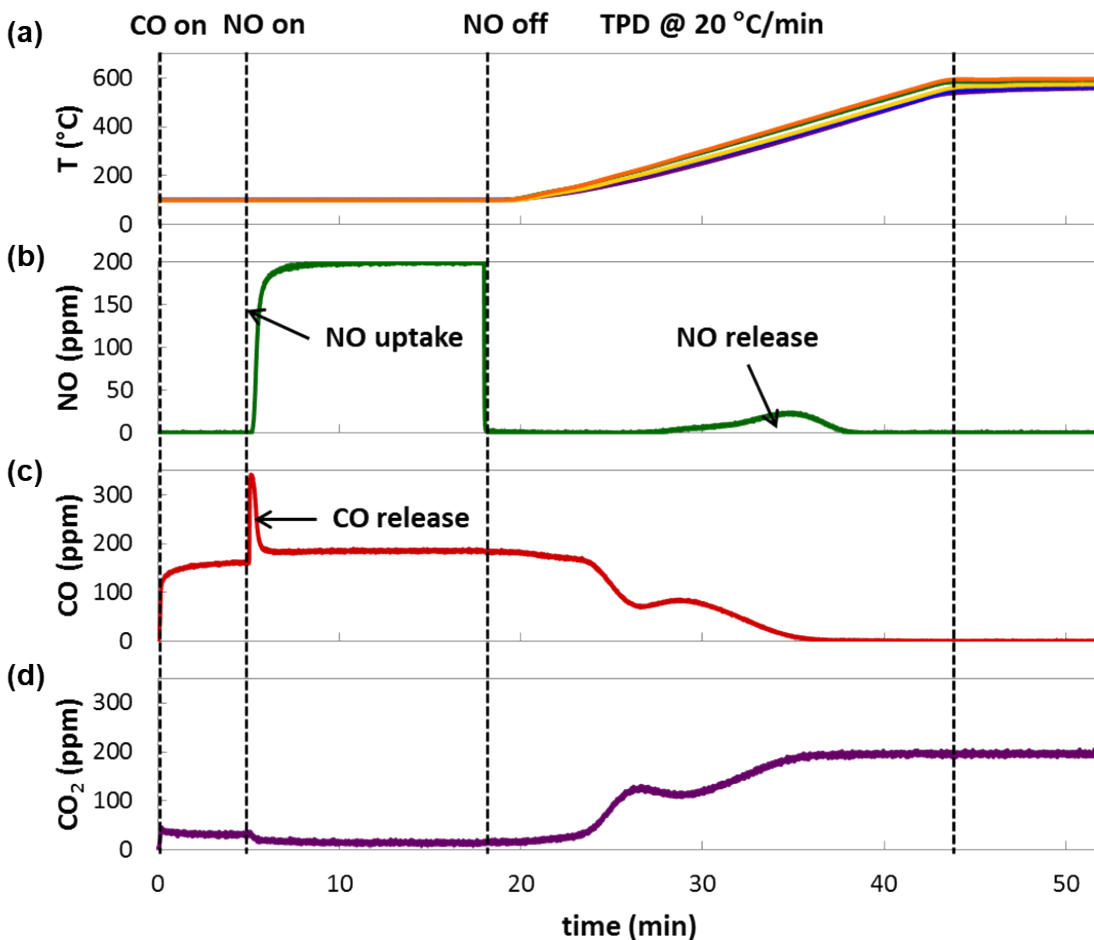


Figure 2: Baseline experimental dataset showing (a) temperature profiles of 5 thermocouples in the reactor, (b) NO concentration profiles, (c) CO concentration profiles, and (d) CO₂ concentration profiles at 100 °C before NO introduction, during isothermal NO adsorption, and during TPD from 100-500 °C. Feed conditions: 200 ppm NO, 200 ppm CO, 10% O₂, 7% H₂O, 0% CO₂, GHSV 30,000 hr⁻¹

3.1. Effect of CO₂

In order to understand the effect of CO₂ concentration on NO storage and release, the concentration of CO₂ was varied from 0 to 13% while keeping the concentrations of the other constituents in the feed constant. In **Figure 3 (a)**, the NO concentration profiles during NO adsorption on the PNA at 100 °C show that the NO uptake rate on the PNA does not change as the CO₂ concentration is varied. Furthermore, as shown in **Figure 3 (b)**, the NO concentration profiles observed during the TPD from 100 to 500 °C, which are indicative of both the NO storage capacity and the stability of the stored NO, also remain unchanged as the CO₂ concentration is increased from 0 to 13%. As CO₂ does not have a significant impact on either the NO uptake rate or the NO

storage capacity of the PNA, it plays no role in the mechanisms for NO storage and release. For the sake of simplicity, CO₂ has been excluded from the feed conditions in the experiments discussed in the following sections.

Since CO₂ concentration has no effect on NO storage and release on the PNA, the data obtained during the six experiments plotted in **Figure 3** provide evidence for the reproducibility of both the experimental apparatus and the PNA material. The agreement between the NO adsorbed quantities is consistent, as well as for the amounts desorbed, for all the experiments presented in this paper. The desorbed quantity being slightly higher than the adsorbed quantity may be due to nonlinearities in the FTIR calibration – the measured NO concentrations during the TPD are quite low (< 25 ppm), and small offsets in the measured concentration integrated over long time periods could add up to the observed difference.

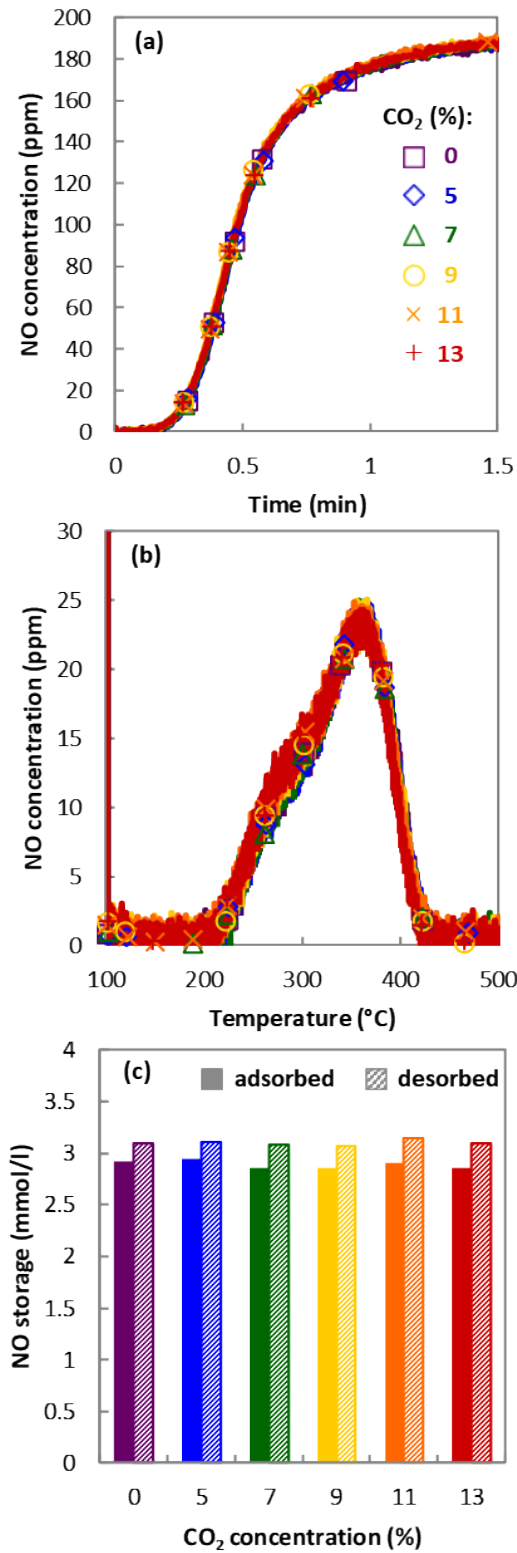


Figure 3: NO concentration profiles during (a) NO adsorption on at 100 °C and (b) TPD from 100-500 °C and, (c) total NO storage measured from NO adsorbed at 100 °C (solid fill) and NO desorbed during TPD from 100-500 °C (diagonal line fill) as the CO₂ concentration is varied in

experiments conducted with Pd/ZSM-5. Feed conditions: 200 ppm NO, 200 ppm CO, 10% O₂, 7% H₂O, 0-13% CO₂, GHSV 30,000 hr⁻¹

3.2. Effect of O₂

The inlet O₂ concentration was varied from 1 to 13% to understand the impact of O₂ on the NO storage and release. As the Pd/ZSM-5 is a model PNA for diesel applications [9], the exhaust composition contained sufficient O₂ in all experiments to maintain net lean operating conditions. The NO concentration profiles during NO exposure to the PNA at 100 °C in **Figure S1 (a)** show that increasing the O₂ concentration from 1 to 13% did not have a significant effect on the NO uptake rate of the PNA. Additionally, the NO concentration profiles during the TPD (data not shown for brevity) from 100 to 500 °C showed minimal variation with the O₂ concentration in the feed. The release profiles showed that the NO storage capacity was essentially unchanged, although the NO was released at slightly lower temperatures as the O₂ concentration was increased. This was a minor effect overall, so variations with O₂ concentration were not considered in the development of the NO storage and release mechanism.

3.3. Effect of NO concentration

In order to understand the impact of NO concentration on the NO storage and release, NO concentration was varied from 25 to 1600 ppm during NO exposure under isothermal conditions at 100 °C. **Figure 4 (a) - (g)** shows that increasing the NO concentration during NO adsorption reduces the time to NO breakthrough. This is not surprising since the available NO storage sites will fill faster at higher NO flux. Interestingly, even at the highest NO concentration, there is still a time period at the beginning of NO exposure during which all the NO is being stored –the rate of NO uptake increases with NO concentration to compensate for the higher levels of NO in the feed gas, **although complete uptake depends on the operating space velocity**. Consistent with this observation, **Figure 4 (h)** shows an apparent first order dependence of NO adsorption rate on NO concentration when the adsorption rates were calculated at 95% storage capacity, i.e., when 95% of available Pd sites are occupied by NO.

Figure 4 (i) shows the integrated NO storage during isothermal adsorption and release during the TPD as the inlet NO concentration was varied. The NO storage capacity of the Pd/ZSM-5 is essentially unchanged even as the NO concentration is varied over two orders of magnitude. Thus, for the adsorption conditions investigated here, the equilibrium between gas phase NO and adsorbed NO lies towards the latter.

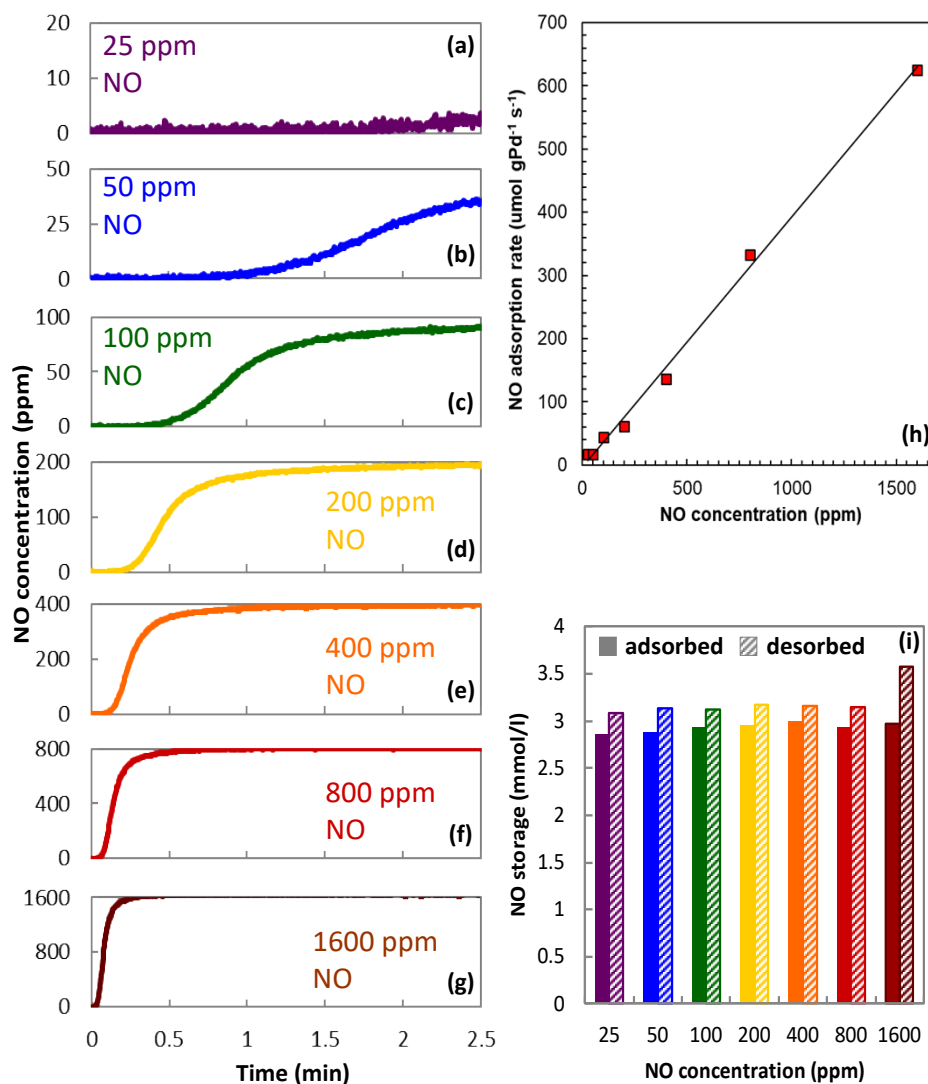


Figure 4: NO concentration profiles during NO adsorption on Pd/ZSM-5 at 100 °C at different NO concentrations (in ppm): (a) 25, (b) 50, (c) 100, (d) 200, (e) 400, (f) 800, (g) 1600, (h) rate of NO adsorption calculated at 95% NO storage capacity as a function of NO concentration and (i) total NO storage as measured from NO adsorbed at 100 °C (solid fill) and NO desorbed during TPD from 100-500 °C (diagonal line fill) as the NO concentration is varied in experiments conducted with Pd/ZSM-5. Feed conditions: **25-1600 ppm NO**, 200 ppm CO, 10% O₂, 7% H₂O, 0% CO₂, GHSV 30,000 hr⁻¹

3.4. Effect of NO adsorption temperature

To understand the impact of NO exposure temperature on the NO storage and release, the NO adsorption temperature was varied from 75 to 225 °C in 25 °C increments. For successful use as part of a diesel aftertreatment system to mitigate cold-start NO_x emissions, ideally, the PNA

should be most effective at trapping NO_x below 200 °C. Beyond this temperature, the urea SCR system can efficiently reduce NO_x emissions under lean conditions. As the feed contained 7% H₂O, 75 °C was selected as the lower limit for the NO adsorption temperature in the current study to prevent the complications of H₂O condensation in the flow reactor.

Consistent with observations reported by Chen et al., the NO concentration profiles during isothermal NO adsorption experiments conducted at adsorption temperatures ranging from 75 to 225 °C in **Figure 5** reveal two distinct trends in the NO uptake on the PNA [9]. As the temperature for NO exposure is increased from 75 to 150 °C, the NO uptake on the PNA increases. On further increase in the NO adsorption temperature from 175 to 225 °C, the NO uptake decreases. **Figure 5 (h)**, which shows the integrated NO uptake and release as a function of adsorption temperature, clearly demonstrates that the NO storage capacity of the Pd/ZSM-5 attained a maximum at 150 °C.

The decrease in NO storage at temperatures above 150 °C is expected, and indeed necessary for the Pd/ZSM-5 to operate as a PNA – the NO stored at low temperatures must be released at higher temperatures for a PNA to be useful. Increasing temperature decreases the stability of the adsorbed NO until the equilibrium reaction favors NO release. **The increase in NO storage at temperatures below 150 °C will be explained** when including the effect of H₂O and Pd dehydration as described in the next section.

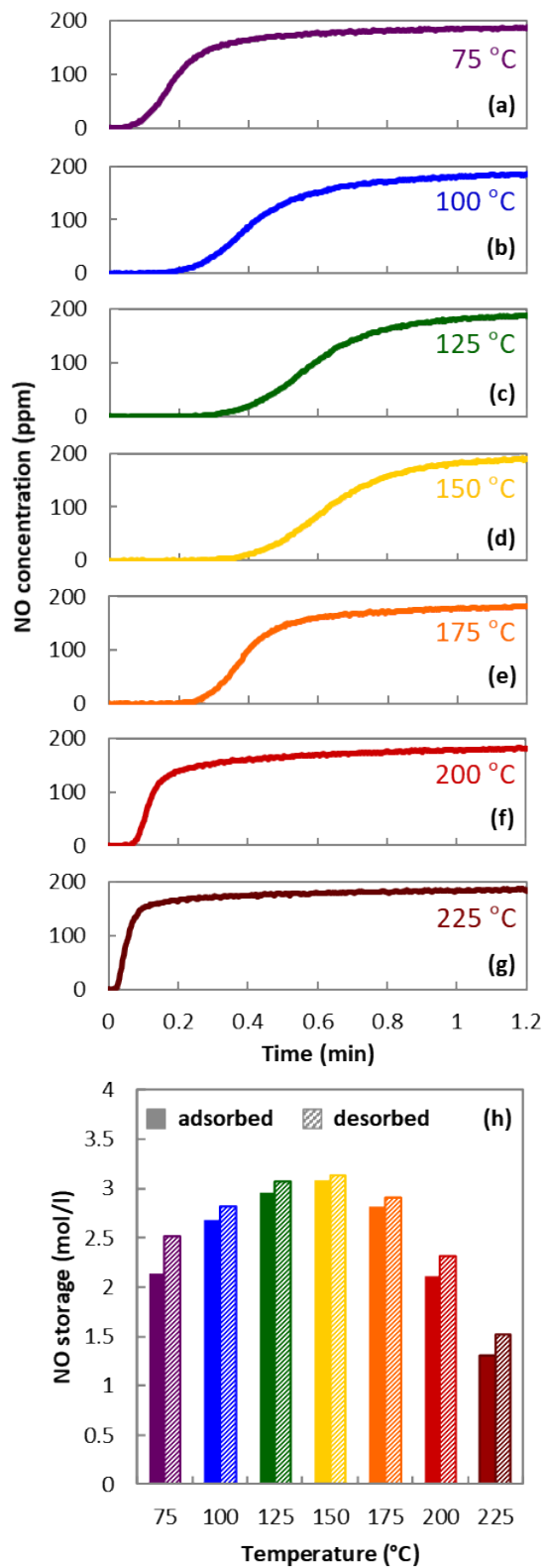


Figure 5: NO concentration profiles during NO adsorption on Pd/ZSM-5 at (a) 75, (b) 100, (c) 125, (d) 150, (e) 175, (f) 200, (g) 225 °C and, (h) total NO storage on the PNA measured from

NO adsorbed (solid fill) and NO desorbed during TPD (diagonal line fill) as the NO adsorption temperature is varied from 75 °C to 225 °C in experiments conducted with Pd/ZSM-5. Feed conditions: 200 ppm NO, 200 ppm CO, 10% O₂, 7% H₂O, 0% CO₂, GHSV 30,000 hr⁻¹

3.5. Effect of H₂O

The impact of H₂O on the NO storage and release was investigated by varying the H₂O concentration in the feed from 5 to 13% during isothermal NO adsorption at 100 °C as well as at 150 °C. From the NO concentration profiles during NO exposure at 100 °C displayed in **Figure 6 (a)**, as the concentration of H₂O in the reaction feed is increased from 5 to 9%, the NO uptake rate decreases. Upon increasing the H₂O concentration in the feed beyond 9%, the NO uptake rate remains unchanged. Interestingly, the wet NO storage (**Figure 6 (b)**) capacity is essentially independent of the H₂O concentration. At the 100 °C adsorption temperature, H₂O appears to slow the kinetics of NO uptake but does not prevent NO from storing at the Pd sites. The lack of an inhibiting effect of increasing H₂O concentration on NO storage capacity seems to contradict observations that were reported by Zheng et al.[12], who saw significant loss in capacity. However, their comparisons were between dry and water-containing conditions. They attributed the loss to competitive adsorption of NO and H₂O on the NO storage sites. Starting with 5% H₂O here, this competition could already be saturated. As observed in **Figure 6 (c)**, when NO is adsorbed on the PNA at 150 °C, varying the H₂O concentration in the feed has minimal impact on the NO uptake rate on the PNA. Furthermore, consistent with findings reported in the earlier section (3.4), the NO uptake rate during isothermal NO exposure is higher at 150 °C for all the H₂O concentrations considered in this study. The H₂O inhibition of the rate of NO uptake at 100 °C is not observed at 150 °C.

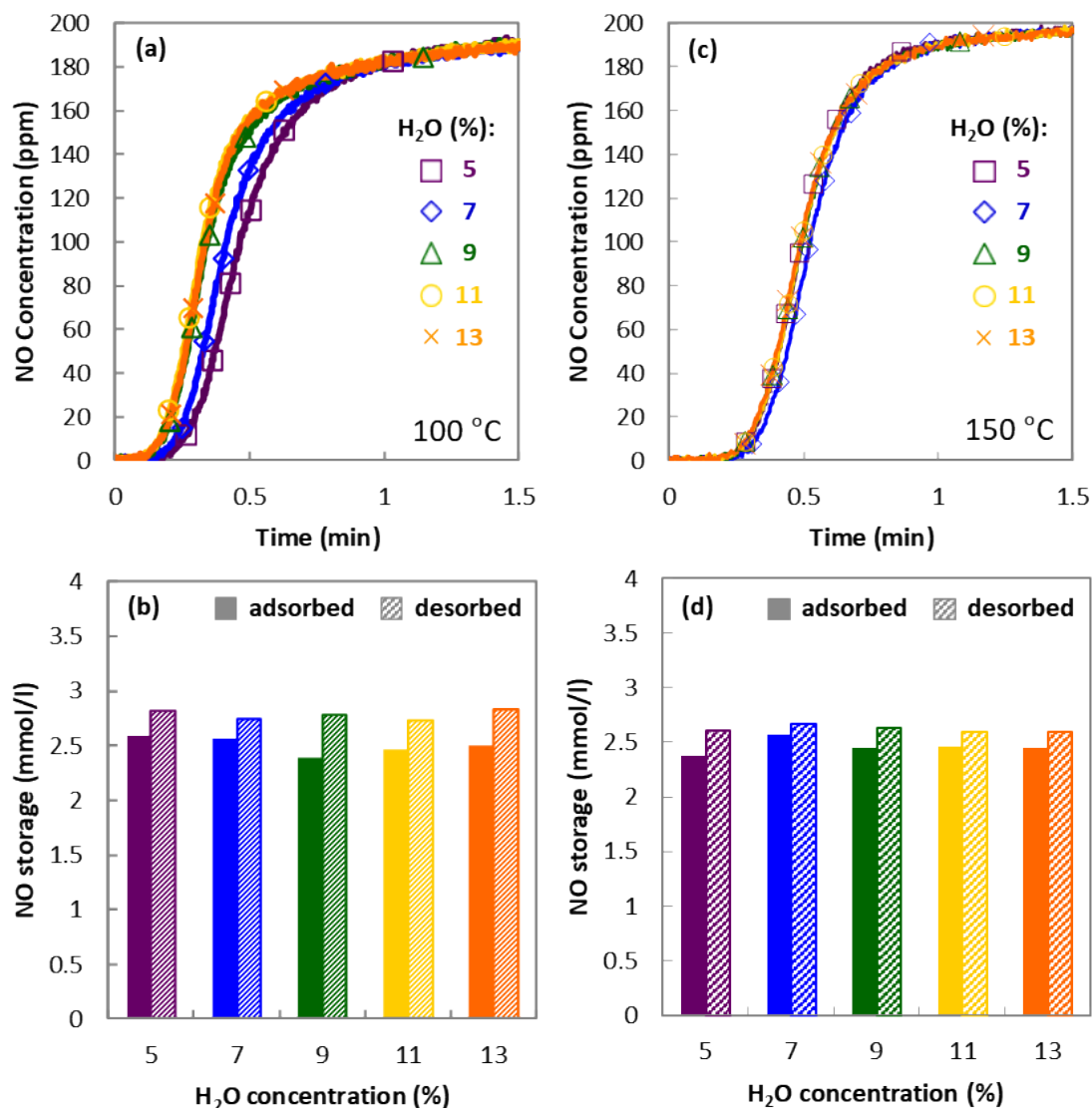


Figure 6: (a) NO concentration profiles during NO adsorption at 100 °C and (b) total NO storage as measured from NO adsorbed at 100 °C (solid fill) and NO desorbed during TPD from 100-500 °C (diagonal line fill); (c) NO concentration profiles during NO adsorption at 150 °C and (d) total NO storage as measured from NO adsorbed at 150 °C (solid fill) and NO desorbed during TPD from 150-500 °C (diagonal line fill) as the H₂O concentration is varied in experiments conducted with Pd/ZSM-5. Feed conditions: 200 ppm NO, 200 ppm CO, 10% O₂, 5-13% H₂O, 0% CO₂, GHSV 30,000 hr⁻¹

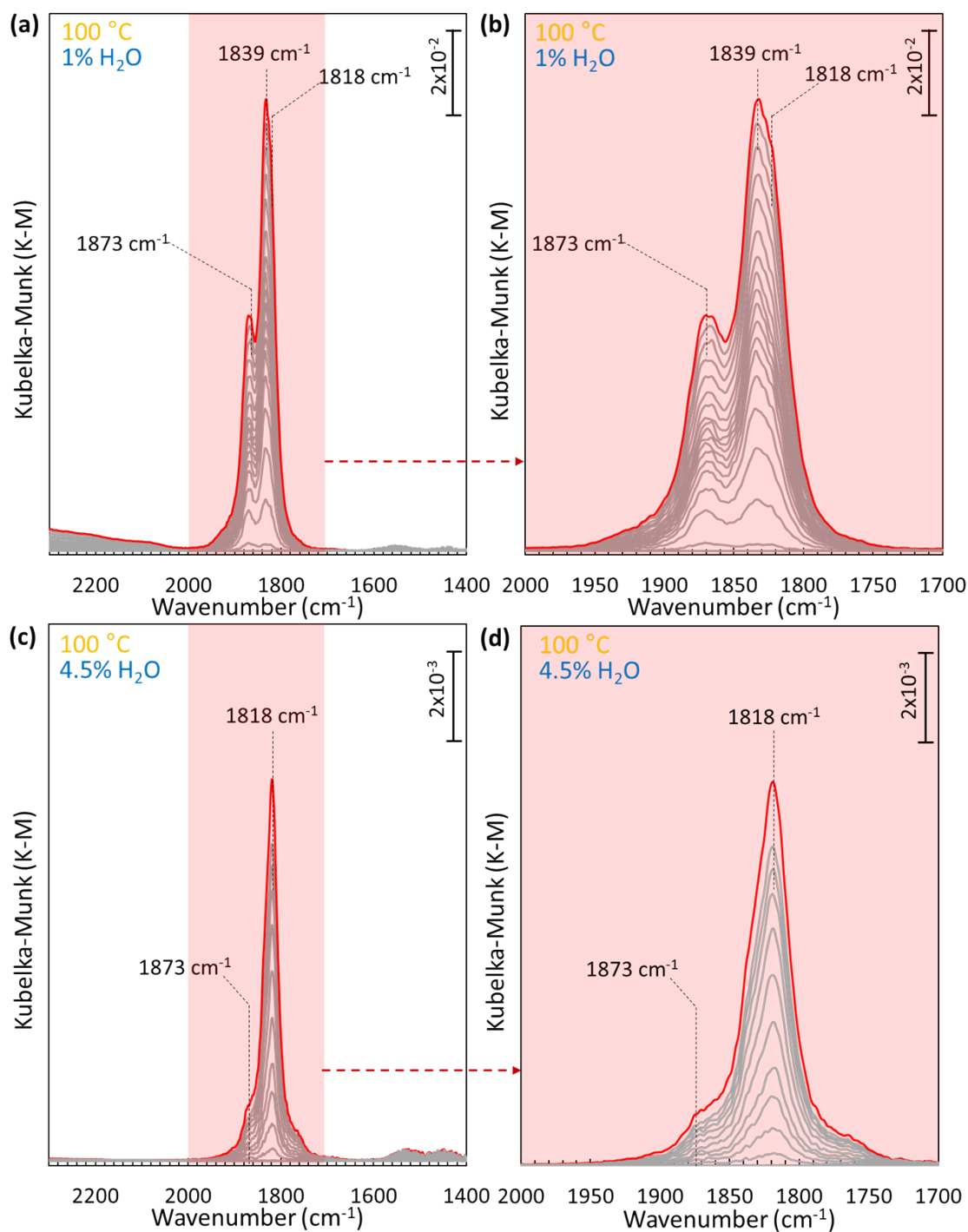
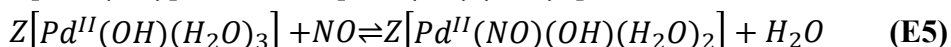
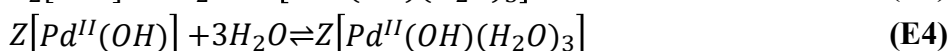
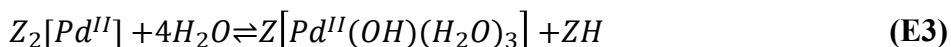


Figure 7: In-situ time-resolved DRIFTS spectra collected at 45 s intervals (final spectrum in red) during NO adsorption on a degreased Pd/ZSM-5 PNA sample at 100 °C in the presence of (a), (b) 1% H₂O and (c), (d) 4.5% H₂O. Feed conditions: 200 ppm NO, 10% O₂, 1% or 4.5% H₂O. Note the scale bars in (c) and (d) are an order of magnitude different compared to (a) and (b).

The formation of hydrated Pd cations in the presence of H₂O has been previously reported to have a significant influence on the nature of Pd species in the PNA, and therefore, the NO adsorption mechanism [21,44,45]. To gain insights into surface intermediates formed on the Pd/ZSM-5 PNA under wet conditions, DRIFTS spectra were collected during NO adsorption at 100 °C in the presence of 1% or 4.5% H₂O. Different from **Figure 3**, the in-situ DRIFTS spectra in **Figure 7** are collected under wet conditions and demonstrate that as the H₂O concentration is increased from 1 to 4.5%, the relative intensity of the peaks at 1873 and 1839 cm⁻¹ associated with Z₂[Pd^{II}(NO)], and Z[Pd^{II}(NO)(OH)], respectively, diminish, accompanied by the simultaneous evolution of a new feature at 1818 cm⁻¹. **Note that even at 1% H₂O, bands associated with NO⁺ (2128 cm⁻¹) and nitrates (~1600 cm⁻¹) disappear.** At 4.5% H₂O, shown in **Figures 7 (c) and (d)**, the peak at 1818 cm⁻¹ dominates the spectra, indicating the evolution of a new Pd-nitrosyl complex and a more uniform Pd speciation within the zeolite. These observations somewhat agree with the results reported in our previous work on Pd/SSZ-13, where we showed that on exposure to NO and H₂O, the formation of Z[Pd^{II}(NO)(H₂O)₃] leading to the shift of N-O stretching frequency to a lower wavenumber. More importantly, when investigating the mobility of the hydrated Pd cations via ab-initio molecular dynamics (AIMD) calculations, we found that Pd cations are solvated by H₂O and detached from the zeolite framework. This effect seems to be independent of zeolite topology. However, the formation of Z[Pd^{II}(NO)(H₂O)₃] involves the migration of Pd cations from a 2Al site to a 1Al site in SSZ-13 along with the oxidation of NO or CO. Although this redox reaction has been reported to result in the transient formation of NO₂ or CO₂ [17,46], in the current study, no transient NO₂ and insignificant transient CO₂ formation was observed in the flow reactor experiments. Hence, we attribute the evolution of the IR feature at 1818 cm⁻¹ to the formation of a similar hydrated Pd-nitrosyl complex, namely, Z[Pd^{II}(NO)(OH)(H₂O)₂]. This variation in Pd speciation is potentially due to the difference in the initial Pd distribution between Pd/ZSM-5 and Pd/SSZ-13 as a result of different Al arrangement within the zeolite. Mechanistically, these results imply that H₂O first reversibly adsorbs on the Pd cations and the addition of NO ultimately leads to the formation of Z[Pd^{II}(NO)(OH)(H₂O)₂]. Considering both Z₂Pd and ZPdOH to start with, this process can be represented by the reactions in equations (E3) - (E5):



Although initially there are two different Pd cationic species indicated by the number of peaks evolved during NO adsorption under dry conditions, **Figure 1**, Pd cations in ZSM-5 zeolite are solvated by H₂O via (E3) and (E4) to maintain a four-fold coordinated structure. Ultimately, after NO is introduced, Z[Pd^{II}(NO)(OH)(H₂O)₂] is formed as the only hydrated Pd-nitrosyl species regardless of the starting Pd species. The combination of reactions (E3) - (E5) also provides

an explanation for the trends in NO adsorption at different adsorption temperatures and is consistent with the 1st order dependence on NO concentration noted in **Figure 4 (h)**. At temperatures below 150 °C, a significant portion of the Pd ions is in a fully hydrated state, which decreases the rate of NO uptake. Increasing the temperature causes some of the H₂O to desorb from the Pd sites, and the NO uptake rate increases. By 150 °C, much of the H₂O has been desorbed from the Pd, and the NO uptake is at its maximum **according to Figure 5**. Since the NO is more strongly adsorbed than the H₂O (otherwise it would not be able to displace the H₂O and adsorb to the Pd), it is likely that the H₂O desorbs prior to the NO during the TPD. This process is summarized in equation (E6) and (E7).

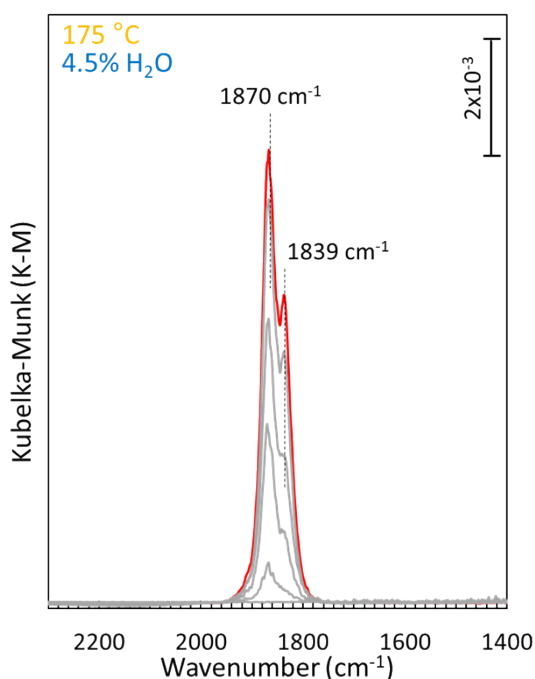
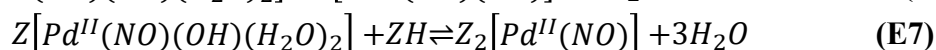
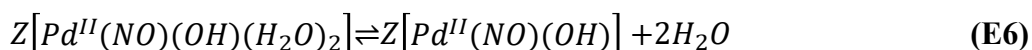


Figure 8: In-situ time-resolved DRIFTS spectra collected at 45 s intervals (final spectrum in red) during NO adsorption on a degreased Pd/ZSM-5 PNA sample at 175 °C in the presence of 4.5% H₂O. Feed conditions: 200 ppm NO, 10% O₂, 4.5% H₂O.

As the flow reactor experiments demonstrated that the effect of H₂O on NO uptake rate depended on the NO adsorption temperature, DRIFTS spectra were also collected during NO adsorption on the Pd/ZSM-5 sample at 175 °C in the presence of 4.5% H₂O to investigate the change in the surface intermediate species at the higher NO adsorption temperature. From **Figure 8** we observe that the peak at 1818 cm⁻¹, which was the main feature at the 100 °C NO adsorption temperature, disappears at 175 °C. Instead, the two spectral peaks at ~ 1873 and 1839 cm⁻¹, which

were previously observed under dry conditions and associated with the $Z_2[Pd^{II}(NO)]$ and $Z[Pd^{II}(OH)(NO)]$ species, reappear. The transition from the hydrated Pd-nitrosyl species (1818 cm^{-1}) at 100 °C to the dehydrated Pd-nitrosyl species (1870 cm^{-1} and 1839 cm^{-1}) at 175 °C supports the hypothesis that H₂O desorbs at a lower temperature than NO and that dehydration of the PNA is facilitated by increasing temperature. Thus, the minimal H₂O inhibition effect on the rate of NO uptake (**Figure 6 (c)**) and the maximized NO storage capacity (**Figure 5 (h)**) at 150 °C observed in the flow reactor experiments, along with the DRIFTS spectra collected during NO adsorption in the presence of 4.5% H₂O at 175 °C (**Figure 8**), indicate the complete dehydration of the PNA at ~150 °C and the formation of dehydrated $Z_2[Pd^{II}(NO)]$ and $Z[Pd^{II}(OH)(NO)]$ species as proposed in reaction equations (E6) and (E7). With the further increase in temperature beyond 150 °C, NO desorption is thermodynamically favored resulting in a decrease in the NO storage capacity of the PNA. This phenomenon is reasonably captured by the reverse reactions in equations (E1) and (E2), which also presents the NO desorption mechanism and leads to the eventual regeneration of the $Z_2[Pd^{II}]$ and $Z[Pd^{II}(OH)]$ species beyond 250 °C.

As the effects of H₂O solvation on Pd speciation and NO adsorption mechanism is captured and discussed, we can now revisit CO oxidation during the TPD. As is discussed with **Figure 2(d)**, there is deviation from a typical CO oxidation light-off curve at ~150°C. Notably, this is the temperature where H₂O desorbs, and the CO_x trace (CO + CO₂) shown in supporting information **Figure S3** suggests that there is no significant CO or CO₂ desorption from previously trapped CO species. We therefore attribute this CO oxidation light-off feature to H₂O desorption and the transition from more active hydrated Pd cations to less active dehydrated Pd cations. The comparison between CO oxidation light-off experiments in the presence and absence of H₂O shown in the supporting information **Figure S4** further confirms that the presence of H₂O significantly shifts the CO oxidation light-off to lower temperatures.

3.6. Effect of CO

The effect of CO concentration on NO storage and release is of significant interest as CO is an integral component of diesel exhaust and has been found to impact the oxidation state of the ion-exchanged Pd NO storage sites within the zeolite [15,25]. Furthermore, other researchers have found that CO promotes NO adsorption on Pd-exchanged zeolites [47]. As noted above (**Figure 2**), all the CO that adsorbs on the Pd/ZSM-5 PNA sample is subsequently released upon introduction of NO, indicating that NO and CO are not co-adsorbed under the experimental conditions examined here. To understand the effect of CO on NO storage and release, both wet and dry conditions have been considered and the results presented in the following sections.

3.6.1. Dry conditions

To gain insights into the effect of CO on NO adsorption on the PNA under dry conditions, NO storage and release was evaluated at 100 °C in the absence of CO and the presence of 200 ppm CO in the feed during NO adsorption. The NO concentration profiles during adsorption under dry conditions in **Figure 9** (curves(a) and (b)) overlay, indicating that the NO uptake rate does not depend on the presence or absence of CO.

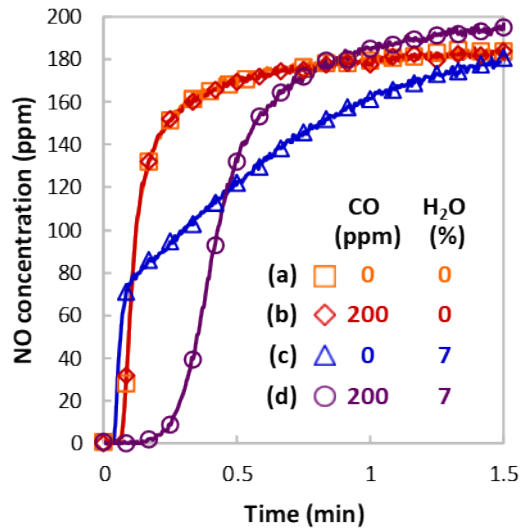


Figure 9: NO concentration profiles during NO adsorption at 100 °C under (a) 0ppm CO, 0% H₂O, (b) 200ppm CO, 0% H₂O, (c) 0 ppm CO, 7% H₂O, and (d) 200 ppm CO, 7% H₂O. Feed conditions: 200 ppm NO, 0 or 200 ppm CO, 10% O₂, 0 or 7% H₂O, 0% CO₂, GHSV 30,000 hr⁻¹

3.6.2. Wet conditions

In contrast to the results under dry conditions, the NO concentration profiles in the presence of H₂O in **Figure 9** (curves (c) and (d)) show that CO has a significant impact on the rate of NO adsorption. In the absence of CO, NO adsorption is slow, and NO breaks through almost immediately after its introduction. After this rapid breakthrough, the NO concentration slowly increases until it reaches the inlet value. In the presence of CO, NO adsorption is much faster, and NO breakthrough is delayed significantly. After breakthrough, the NO concentration increases to the inlet level faster than in the absence of CO. The total NO storage is very similar with and without CO, but the rates of NO adsorption are quite different.

The effect of CO on NO storage and release under wet conditions (7% H₂O) was further investigated by varying the CO concentration in the feed from 50 to 800 ppm CO during NO adsorption at 100 °C. The NO concentration profiles in **Figure 10 (a)** show that, as the CO concentration is increased, the NO uptake rate increases up to ~ 400 ppm CO. Further increasing the CO concentration to 800 ppm has minimal impact on the NO uptake rate. The rate differences can be seen in the crossover of the NO concentration profiles in **Figure 10 (a)**: at 800 ppm CO, the NO breakthrough occurs much later than at the lower CO concentrations, but the NO concentration more rapidly approaches the inlet value; at 50 ppm CO, the NO breakthrough occurs earlier, but the approach to the inlet NO concentration occurs more slowly, indicating that the Pd/ZSM-5 is storing more NO at later adsorption times. The total NO stored during both adsorption and release in **Figure 10 (b)** shows only a small effect of changing CO concentration. Thus, as with H₂O at 100 °C, the primary impact of changing CO concentration appears to be on the rate of

NO adsorption on the Pd sites rather than the total amount of NO that can be stored at those sites. **Figure 9** showed that CO had no effect on NO adsorption under dry conditions, while **Figures 10 (a) and (b)** showed that increasing CO increases the rate of NO adsorption in the presence of H₂O at 100 °C. The next logical step was to evaluate the effects of CO concentration on NO adsorption at 150 °C, with results shown in **Figure 10 (c)**. Interestingly, varying CO concentration from 50 to 400 ppm had minimal effect on either the rate of NO adsorption in **Figure 10 (c)** or the total NO stored in **Figure 10 (d)**. Further increasing CO concentration to 800 ppm caused a small decrease in total NO stored, which is also apparent in earlier NO breakthrough.

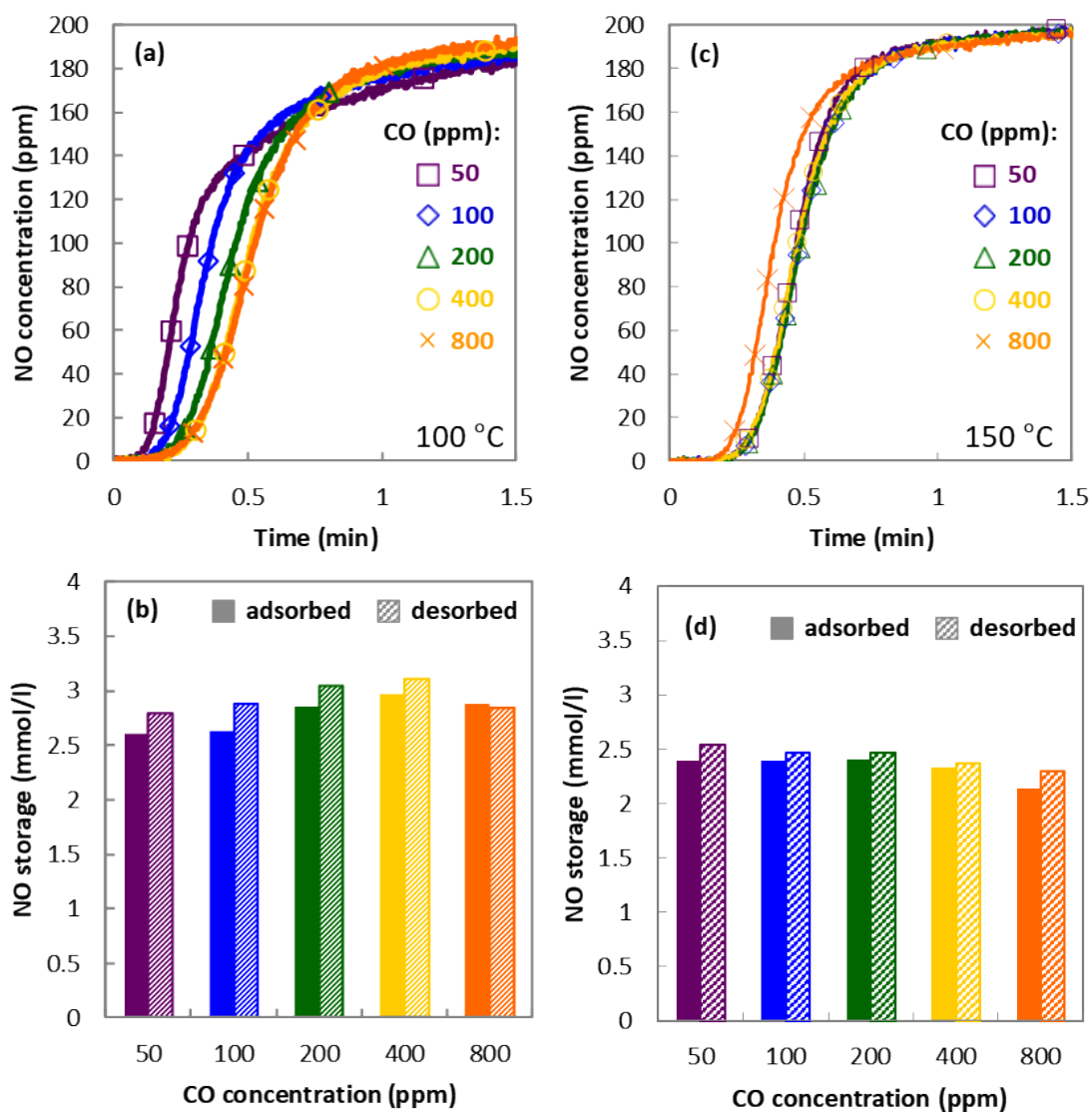
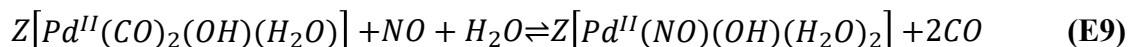
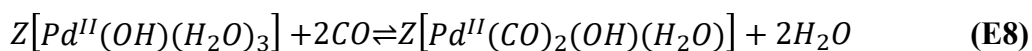


Figure 10: (a) NO concentration profiles during NO adsorption at 100 °C and (b) total NO storage as measured from NO adsorbed at 100 °C (solid fill) and NO desorbed during TPD from 100-500 °C (diagonal line fill); (c) NO concentration profiles during NO adsorption at 150 °C and (d) total NO storage as measured from NO adsorbed at 150 °C (solid fill) and NO desorbed during TPD from 150-500 °C (diagonal line fill) as the CO concentration is varied in experiments conducted with Pd/ZSM-5. Feed conditions: 200 ppm NO, **50-800 ppm CO**, 10% O₂, 7% H₂O, 0% CO₂, GHSV 30000 hr⁻¹

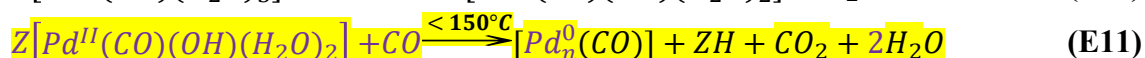
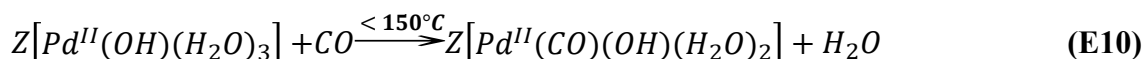
Considering that CO increases the rate of NO uptake in the presence of H₂O at 100 °C, but has no appreciable effect on NO storage under dry conditions or in the presence of H₂O at 150 °C, CO only impacts NO storage under conditions where the Pd is in a hydrated state. It is therefore proposed that CO helps mitigate the slow uptake of NO in the presence of elevated H₂O concentrations by displacing some of the water from the Pd sites before the NO is introduced, which can be described by equations (E8) and (E9):



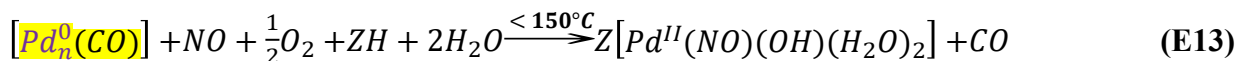
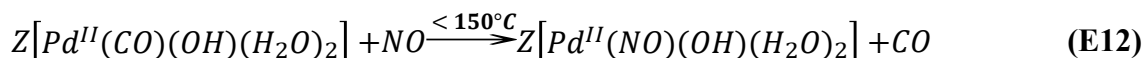
CO displacement by NO is a faster process than H₂O displacement by NO, thus NO adsorption is accelerated in the presence of CO. To further prove the competitive adsorption process and to investigate the interaction between CO and NO on the surface of the Pd/ZSM-5 PNA at 100 °C, in-situ DRIFTS experiments were conducted. C-O stretching peaks at 2144, 2140, 2122, and 2108 cm⁻¹ assigned to di-carbonyl and mono-carbonyl species coordinated with Pd²⁺ cations, and a feature at 1966 cm⁻¹ associated with CO on reduced Pd particles were observed when CO was adsorbed on Pd/ZSM-5 under dry conditions as shown in **Figure 11 (a)** [12,44]. Multiple vibrational frequencies associated with well identified Pd-carbonyl species observed in the 2100 to 2200 cm⁻¹ region further support the previously mentioned heterogeneity of Pd²⁺ cations in ZSM-5 due to the random Al distribution and the complex ion-exchange positions. However, when 4.5% H₂O was introduced to the system, from **Figure 11 (b)** we observe that the features at 2144, 2140, 2122 and 2108 cm⁻¹ disappear due to hydration of Pd²⁺ cations, and the evolution of two features at 2132 and 2117 cm⁻¹ indicating the formation of a different Pd-dicarbonyl species and a more homogeneous-like Pd speciation within ZSM-5. This phenomenon is similar to what has been observed with NO adsorption and agrees well with the proposed reaction (E8). More specifically, Pd cations are first solvated by H₂O and form the same dicarbonyl species after CO adsorption despite different starting Pd species. With an Ar purge, however, the features at 2132 and 2117 cm⁻¹ disappear demonstrating the instability of the Pd²⁺- dicarbonyl species formed in the presence of H₂O.

The peak at 1960 cm⁻¹ in the C-O stretching region, which dominates the DRIFTS spectra under wet conditions, is typically associated with CO adsorbed on metallic Pd particles [48–51]. The intensity of this peak is significantly higher than the corresponding peak at 1966 cm⁻¹ under dry conditions suggesting the formation of reduced Pd⁰ clusters (indicated as Pd⁰_n) when H₂O and CO are both present. Another possibility is that this feature is still associated with mono-carbonyl species bound to hydrated Pd²⁺ cations. Hydration leading to a 60 cm⁻¹ peak shift in N-O stretching frequency for Pd/SSZ-13 and a similar influence of H₂O on the C-O stretching frequency of mono-carbonyl species in Pd/BEA has been previously reported [21,44]. As the hydration of mono-carbonyl species can lead to a significant peak shift to lower wavenumbers, the peak at 1966 cm⁻¹ could be assigned to $Z[Pd^{II}(CO)(OH)(H_2O)_2]$ where Pd remains in the 2+

oxidation state [21]. With the evidence we have, we cannot definitively assign this IR feature to one or the other of these two possibilities, although literature and Pd mobility aspects suggest it is the formation of small Pd clusters that leads to this peak appearing, and 1960 cm⁻¹ seems to be too low of a wavenumber to be mono-carbonyl species bound to Pd cations. Nevertheless, both proposed CO adsorption mechanisms demonstrate significant differences in surface environment and Pd speciation upon CO exposure indicating that the formation of Pd-carbonyl species or small Pd clusters plays an important role in mitigating the H₂O inhibition effect by CO observed on the PNA during NO adsorption below 150 °C. We introduce reaction equations (E10) and (E11) as two possible pathways besides (E8) and (E9) that mitigate the H₂O inhibition effect on the rate of NO adsorption by CO:



After saturation with CO in the presence of 4.5% H₂O, background spectra were collected and subtracted following which NO was introduced to the DRIFTS cell at 100 °C. From the DRIFTS spectra collected during NO adsorption at 100 °C under wet conditions shown in **Figure 11 (d)**, we observe the evolution of the hydrated mono-nitrosyl Pd species (1818 cm⁻¹), accompanied by the simultaneous appearance of negative peaks corresponding to hydrated di-carbonyl Pd complexes (2122 and 2132 cm⁻¹) indicating the desorption of CO as soon as Pd/ZSM-5 is exposed to NO, which is captured by (E9). The negative feature at 1960 cm⁻¹ suggests either the loss of the mono-carbonyl species bound to Pd or CO adsorbed on small Pd clusters, all of which indicates, again, the desorption of CO and can be presented by equations (E12) and (E13). Note, the negative 1960 cm⁻¹ feature does not demonstrate NO adsorption on the reduced Pd clusters because the single peak at 1818 cm⁻¹ suggests the formation of previously assigned of $Z[Pd^{II}(NO)(H_2O)_3]$ only. Instead, these results indicate that even if Pd clusters are formed during the CO + H₂O exposure, addition of NO will lead to the desorption of CO and a subsequent or simultaneous redispersion of Pd clusters back into the cation form in the presence of O₂.



While prior literature reported the formation of a co-adsorbed CO and NO carbonyl-nitrosyl Pd complex on a Pd/SSZ-13 PNA under dry conditions [47], we did not observe the corresponding IR feature and have no evidence to support the existence of co-adsorbed carbonyl-nitrosyl species in the presence of H₂O on the Pd/ZSM-5 sample. The formation of $Z[Pd^{II}(NO)(OH)(H_2O)_2]$ species indicated by the peak at 1818 cm⁻¹ in **Figure 11 (d)**, along with the disappearance of the

peaks in the C-O stretching region with introduction of NO to Pd/ZSM-5, suggests replacement of CO by NO in the hydrated Pd complex. Furthermore, this is consistent with recent work with Pd/FER, where NO displaced CO from this type of PNA sample as well [52].

Based on the IR results and trends shown in **Figure 10**, equations (E8) - (E13) above capture the mitigation of the H₂O inhibition effect by CO on the PNA at NO adsorption temperatures lower than 150 °C as well as the CO release on introduction of NO to the PNA. Again, CO adsorption on hydrated Pd cations forming mono-carbonyl species and the subsequent NO adsorption represented by (E10) and (E12) can be replaced or occur in parallel to the reversible formation of small Pd clusters represented by (E11) and (E13).

Note that for NO exposure temperatures ≥ 150 °C neither H₂O nor CO has a significant impact on NO storage and release, and equations (E1) and (E2) are sufficient to describe the NO adsorption and desorption process.

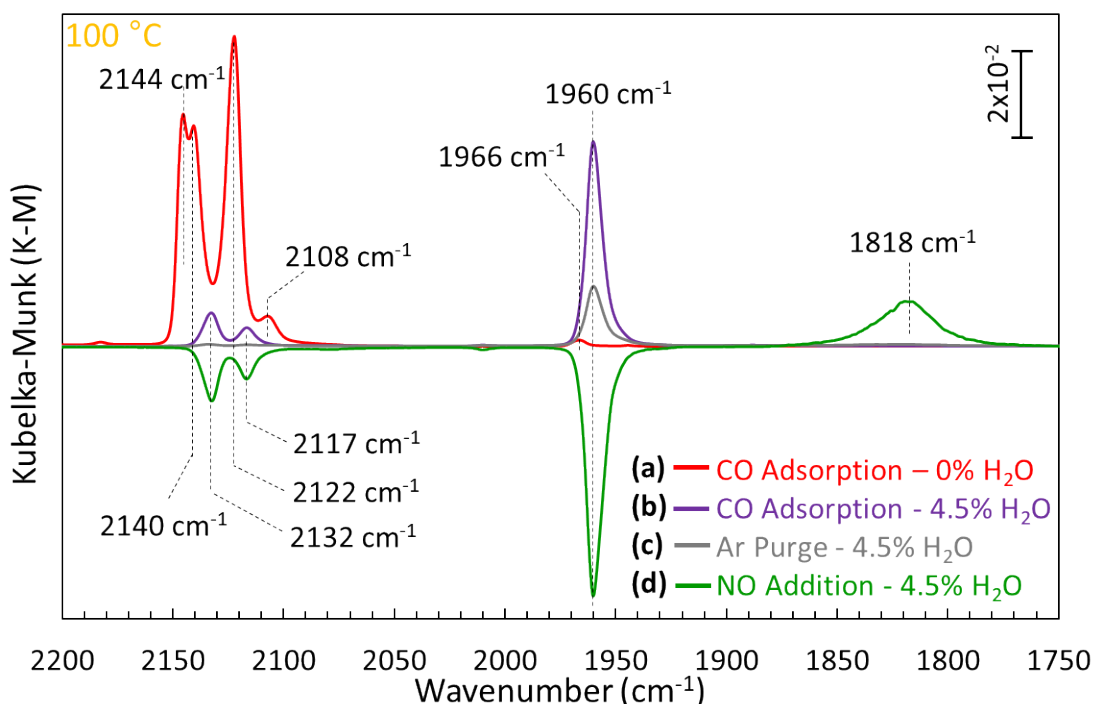


Figure 11: In-situ DRIFTS spectra collected on a degreened Pd/ZSM-5 PNA sample at 100 °C under (a) dry conditions with 200 ppm CO, and in the presence of 4.5% H₂O with (b) 200 ppm CO, followed by (c) Ar purge and (d) 200 ppm NO exposure. Feed conditions: 0-200 ppm NO, 10% O₂, 0-4.5% H₂O, 0-200 ppm CO.

3.7. Effect of order of introduction of NO and CO to the PNA under wet conditions

For the results presented in the previous sections, the baseline condition consisted of exposing the PNA to CO for five minutes before NO. To investigate if the order of introduction of NO and CO to the PNA under wet conditions at 100 °C had an impact on the NO storage and

release, two additional cases were considered: (i) simultaneous introduction of NO and CO and (ii) introduction of NO before CO. On comparing the NO concentration profiles during NO adsorption at 100 °C for the three modes in **Figure 12 (a)**, we observe that the NO adsorption rate is much faster when CO is introduced first, resulting in a longer delay before NO breakthrough. However, the corresponding NO release profiles during TPD from 100 to 500 °C in **Figure 12 (b)** show that the NO storage capacity remains unchanged irrespective of the mode of introduction of NO and CO to the PNA, showing once again that the role of CO is to increase the rate of NO adsorption, but not the total amount stored.

The slow NO adsorption rate when CO and NO are introduced simultaneously show that CO must have sufficient time to displace some of the H₂O from the Pd sites. The adsorption of CO itself is not inherently faster than NO adsorption; the 5 min CO exposure time prior to NO introduction used in most of the experiments here gives enough time for the CO to displace some of the H₂O and adsorb to the Pd sites. When NO is introduced, it rapidly displaces the CO from the Pd sites.

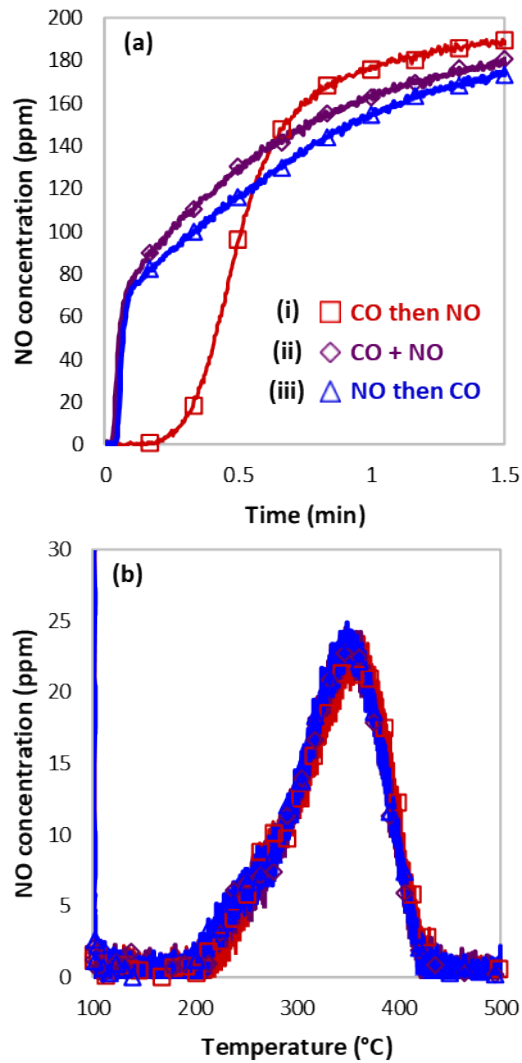


Figure 12: NO concentration profiles during (a) NO adsorption at 100 °C and (b) TPD (100-500 °C) when (i) CO is introduced before NO, (ii) CO and NO are simultaneously introduced and (iii) NO is introduced before CO to the PNA. Feed conditions: 200 ppm NO, 200 ppm CO, 10% O₂, 0% H₂O, 0% CO₂, GHSV 30,000 hr⁻¹

3.8. Preliminary mechanism

A proposed mechanism for PNA NO adsorption and release under wet conditions capturing the observed trends is shown in **Figure 13**. Starting with Pd²⁺ in the Pd ion-exchanged ZSM-5, the mechanism captures (1) adsorption of H₂O at operating temperatures <150 °C and (2) resulting inhibition of the NO adsorption rate on hydrated Pd²⁺; (3) CO displacement of adsorbed H₂O on Pd²⁺; (4) fast CO displacement by NO, thereby mitigating H₂O inhibition on the rate of NO adsorption; (5) the absence of H₂O or CO effects at adsorption temperatures ≥150 °C; (6) desorption of H₂O as the temperature is increased above 150 °C; and (7) NO release from the Pd²⁺ storage sites as the temperature is increased beyond 250 °C.

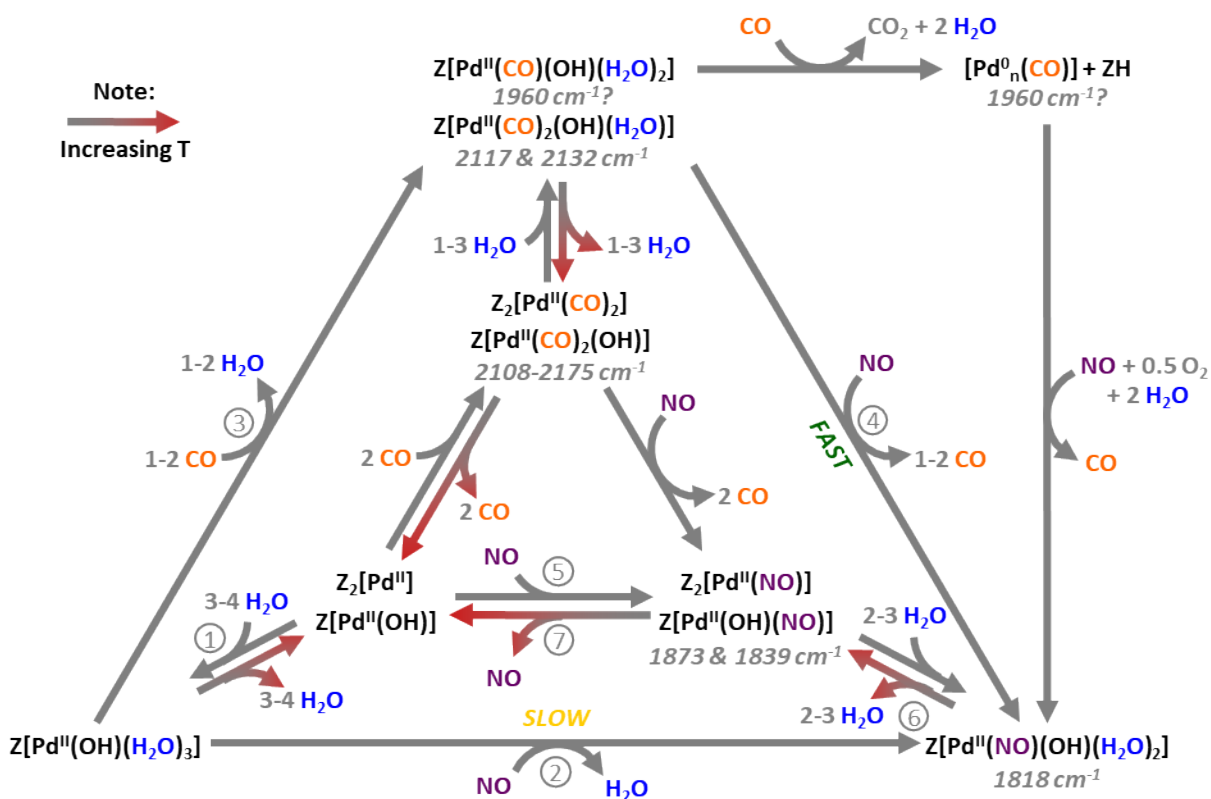


Figure 13: Proposed mechanism for NO adsorption and release on Pd/ZSM-5 based on flow reactor experiments capturing key gas composition and temperature effects as well as identification of surface intermediates through DRIFTS. The arrows shaded red on one end indicate increasing temperature. **The circled numbers correspond to the observations summarized in the text.**

4. Conclusions

A systematic flow reactor and IR characterization study was conducted to understand the impact of operating conditions on Pd/ZSM-5 NO storage and release. Observations include the following.

- Changes in CO₂ and O₂ concentration have minimal effect on NO adsorption and release.
- Although NO concentration does not impact total NO storage capacity, it does impact the rate of NO adsorption.
- NO storage capacity increased from 75 to 150 °C, and decreased from 150 to 225 °C, and this trend is related to the combined effects of Pd hydration/dehydration and stability of adsorbed NO.
- Also related to Pd hydration, at temperatures <150 °C, increasing H₂O concentration decreases NO adsorption rate, while at temperatures ≥150 °C, changing H₂O concentration has no effect on NO adsorption/desorption.
- At temperatures <150 °C, CO mitigates the H₂O inhibition of NO adsorption by displacing some of the H₂O on the Pd storage sites, but CO has no effect under dry conditions or at temperatures ≥150 °C due to Pd dehydration.
- NO rapidly displaces CO from the Pd sites; NO+CO co-adsorption is not observed on Pd/ZSM-5 under the conditions used in this study.
- NO concentration effect and CO inclusion results highlight the importance of looking at not just total NO storage capacities but also rates of NO adsorption with PNA materials; if adsorption rates are too low, the PNA materials will not effectively trap NO during the highly transient operating conditions associated with engine cold start conditions.

Lastly, a mechanism for NO adsorption and desorption on Pd/ZSM-5 is proposed, which captures these observations and includes key surface intermediates identified through DRIFTS experiments. This mechanism provides a foundation for future PNA performance modeling efforts.

5. Acknowledgements

This research was supported by the DOE Office of Energy Efficiency and Renewable Energy (EERE) and Vehicle Technologies Office (VTO) and used resources at the National Transportation Research Center, a DOE-EERE User Facility at Oak Ridge National Laboratory, under the Cross-cut Lean Exhaust Emissions Reduction Simulations (CLEERS) initiative. The authors gratefully acknowledge guidance and support from Ken Howden, Siddiq Khan, and Gurpreet Singh at DOE VTO and Hai-Ying Chen at Johnson Matthey.

6. References

- [1] F. Gramigni, T. Sella, I. Nova, E. Tronconi, Catalyst systems for selective catalytic reduction + NO: X trapping: From fundamental understanding of the standard SCR reaction to practical applications for lean exhaust after-treatment, *React. Chem. Eng.* 4 (2019) 1165–1178.
- [2] C.K. Lambert, Perspective on SCR NO_x control for diesel vehicles, *React. Chem. Eng.* 4 (2019) 969–974.
- [3] A.M. Beale, F. Gao, I. Lezcano-Gonzalez, C.H.F. Peden, J. Szanyi, Recent advances in automotive catalysis for NO_x emission control by small-pore microporous materials, *Chem. Soc. Rev.* 44 (2015) 7371–7405.
- [4] M.P. Harold, NO_x storage and reduction in lean burn vehicle emission control: A catalytic engineer's playground, *Curr. Opin. Chem. Eng.* 1 (2012) 303–311.

- [5] H.Y. Chen, S. Mulla, E. Weigert, K. Camm, T. Ballinger, J. Cox, P. Blakeman, Cold start concept (CSCTM): A novel catalyst for cold start emission control, SAE Tech. Pap. 2 (2013) 372–381.
- [6] Y. Gu, W.S. Epling, Passive NO_x adsorber: An overview of catalyst performance and reaction chemistry, *Appl. Catal. A Gen.* 570 (2019) 1–14.
- [7] M. Moliner, A. Corma, From metal-supported oxides to well-defined metal site zeolites: The next generation of passive NO_x adsorbers for low-temperature control of emissions from diesel engines, *React. Chem. Eng.* 4 (2019) 223–234.
- [8] J. Lee, J.R. Theis, E.A. Kyriakidou, Vehicle emissions trapping materials: Successes, challenges, and the path forward, *Appl. Catal. B Environ.* 243 (2019) 397–414.
- [9] H.-Y. Chen, D. Liu, E. Weigert, L. Cumaranatunge, K. Camm, P. Bannon, J. Cox, L. Arnold, Durability Assessment of Diesel Cold Start Concept (dCSCTM) Technologies, SAE Int. J. Engines. 10 (2017) 2017-01–0955.
- [10] J.R. Theis, C.K. Lambert, An assessment of low temperature NO_x adsorbers for cold-start NO_x control on diesel engines, *Catal. Today.* 258 (2015) 367–377.
- [11] J. Lee, Y. Ryou, S.J. Cho, H. Lee, C.H. Kim, D.H. Kim, Investigation of the active sites and optimum Pd/Al of Pd/ZSM-5 passive NO adsorbers for the cold-start application: Evidence of isolated-Pd species obtained after a high-temperature thermal treatment, *Appl. Catal. B Environ.* 226 (2018) 71–82.
- [12] Zheng, Y.; Kovarik, L.; Engelhard, M. H.; Wang, Y.; Wang, Y.; Gao, F.; Szanyi, J. Low-Temperature Pd/Zeolite Passive NO_x Adsorbers: Structure, Performance, and Adsorption Chemistry. *J. Phys. Chem. C* 2017, 121 (29), 15793–15803.
- [13] Wang, A.; Xie, K.; Kumar, A.; Kamasamudram, K.; Olsson, L. Layered Pd/SSZ-13 with Cu/SSZ-13 as PNA – SCR Dual-Layer Monolith Catalyst for NO_x Abatement. *Catal. Today* 2021, 360, 356–366.
- [14] Y. Ryou, J. Lee, S.J. Cho, H. Lee, C.H. Kim, D.H. Kim, Activation of Pd/SSZ-13 catalyst by hydrothermal aging treatment in passive NO adsorption performance at low temperature for cold start application, *Appl. Catal. B Environ.* 212 (2017) 140–149.
- [15] Y. Ryou, J. Lee, Y. Kim, S. Hwang, H. Lee, C.H. Kim, D.H. Kim, Effect of reduction treatments (H₂ vs. CO) on the NO adsorption ability and the physicochemical properties of Pd/SSZ-13 passive NO_x adsorber for cold start application, *Appl. Catal. A Gen.* 569 (2019) 28–34.
- [16] H.-Y. Chen, J.E. Collier, D. Liu, L. Mantarosie, D. Durán-Martín, V. Novák, R.R. Rajaram, D. Thompsett, Low Temperature NO Storage of Zeolite Supported Pd for Low Temperature Diesel Engine Emission Control, *Catal. Letters.* 146 (2016) 1706–1711.
- [17] A. Gupta, S.B. Kang, M.P. Harold, NO_x uptake and release on Pd/SSZ-13: Impact Of Feed composition and temperature, *Catal. Today.* 360 (2021) 411–425.
- [18] Mihai, O.; Trandafilović, L.; Wentworth, T.; Torres, F. F.; Olsson, L. The Effect of Si/Al Ratio for Pd/BEA and Pd/SSZ-13 Used as Passive NO_x Adsorbers. *Top. Catal.* 2018, 61 (18–19), 2007–2020.
- [19] Porta, A.; Pellegrinelli, T.; Castoldi, L.; Matarrese, R.; Morandi, S.; Dzwigaj, S.; Lietti, L. Low Temperature NO_x Adsorption Study on Pd-Promoted Zeolites. *Top. Catal.* 2018, 61 (18–19), 2021–2034.
- [20] J. Lee, Y. Ryou, S. Hwang, Y. Kim, S.J. Cho, H. Lee, C.H. Kim, D.H. Kim, Comparative study of the mobility of Pd species in SSZ-13 and ZSM-5, and its implication for their activity as passive NO_x adsorbers (PNAs) after hydro-thermal aging, *Catal. Sci. Technol.* 9

- (2019) 163–173.
- [21] D. Mei, F. Gao, J. Szanyi, Y. Wang, Mechanistic insight into the passive NO_x adsorption in the highly dispersed Pd/HBEA zeolite, *Appl. Catal. A Gen.* 569 (2019) 181–189.
- [22] M. Ambast, K. Karinshak, B.M.M. Rahman, L.C. Grabow, M.P. Harold, Passive NO_x adsorption on Pd/H-ZSM-5: Experiments and modeling, *Appl. Catal. B Environ.* 269 (2020) 118802.
- [23] T.M. Lardinois, J.S. Bates, H.H. Lippie, C.K. Russell, J.T. Miller, H.M. Meyer, K.A. Unocic, V. Prikhodko, X. Wei, C.K. Lambert, A.B. Getsoian, R. Gounder, Structural Interconversion between Agglomerated Palladium Domains and Mononuclear Pd(II) Cations in Chabazite Zeolites, *Chem. Mater.* 33 (2021) 1698–1713.
- [24] C. Liu, J. Wang, Z. Chen, J. Wang, M. Shen, Improvement of NO_x uptake/release over Pd/Beta by propylene: shielding effect of intermediates on adsorbed NO_x species, *Phys. Chem. Chem. Phys.* 23 (2021) 5261–5269.
- [25] Y. Gu, R.P. Zelinsky, Y.-R. Chen, W.S. Epling, Investigation of an irreversible NO_x storage degradation Mode on a Pd/BEA passive NO_x adsorber, *Appl. Catal. B Environ.* 258 (2019) 118032.
- [26] Y. Murata, T. Morita, K. Wada, H. Ohno, NO_x Trap Three-Way Catalyst (N-TWC) Concept: TWC with NO_x Adsorption Properties at Low Temperatures for Cold-Start Emission Control, *SAE Int. J. Fuels Lubr.* 8 (2015) 454–459.
- [27] C. Descorme, P. Gélin, M. Primet, C. Lécuyer, Infrared study of nitrogen monoxide adsorption on palladium ion-exchanged ZSM-5 catalysts, *Catal. Letters.* 41 (1996) 133–138.
- [28] B. Pommier, P. Gélin, On the nature of Pd species formed upon exchange of H-ZSM-5 with Pd(NH₃)₄²⁺ and calcination in O₂, *Phys. Chem. Chem. Phys.* 1 (1999) 1665–1672.
- [29] K. Okumura, J. Amano, N. Yasunobu, M. Niwa, X-ray Absorption Fine Structure Study of the Formation of the Highly Dispersed PdO over ZSM-5 and the Structural Change of Pd Induced by Adsorption of NO, *J. Phys. Chem. B.* 104 (2000) 1050–1057.
- [30] B. Pommier, P. Gelin, Infrared and volumetric study of NO adsorption on Pd-H-ZSM-5, *Phys. Chem. Chem. Phys.* 3 (2001) 1138–1143.
- [31] K. Khivantsev, N.R. Jaegers, L. Kovarik, J.C. Hanson, F. (Feng) Tao, Y. Tang, X. Zhang, I.Z. Koleva, H.A. Aleksandrov, G.N. Vayssilov, Y. Wang, F. Gao, J. Szanyi, Achieving Atomic Dispersion of Highly Loaded Transition Metals in Small-Pore Zeolite SSZ-13: High-Capacity and High-Efficiency Low-Temperature CO and Passive NO_x Adsorbers, *Angew. Chemie Int. Ed.* 57 (2018) 16672–16677.
- [32] A. Vu, J. Luo, J. Li, W.S. Epling, Effects of CO on Pd/BEA Passive NO_x Adsorbers, *Catal. Letters.* 147 (2017) 745–750.
- [33] Chen, Z.; Wang, M.; Wang, J.; Wang, C.; Wang, J.; Li, W.; Shen, M. Investigation of Crystal Size Effect on the NO_x Storage Performance of Pd/SSZ-13 Passive NO_x Adsorbers. *Appl. Catal. B Environ.* 2021, 291 (January), 120026.
- [34] S. Sinha Majumdar, J.A. Pihl, T.J. Toops, Reactivity of novel high-performance fuels on commercial three-way catalysts for control of emissions from spark-ignition engines, *Appl. Energy.* 255 (2019) 113640.
- [35] S. Sinha Majumdar, J.A. Pihl, Impact of Selected High-Performance Fuel Blends on Three-Way Catalyst Light Off under Synthetic Spark-Ignition Engine-Exhaust Conditions, *Energy & Fuels.* (2020).
- [36] Theis, J. R.; Ura, J. A. Assessment of Zeolite-Based Low Temperature NO_x Adsorbers: Effect of Reductants during Multiple Sequential Cold Starts. *Catal. Today* 2021, 360, 340–

- 349.
- [37] Gu, Y.; Marino, S.; Cortés-Reyes, M.; Pieta, I. S.; Pihl, J. A.; Epling, W. S. Integration of an Oxidation Catalyst with Pd/Zeolite-Based Passive NO_x Adsorbers: Impacts on Degradation Resistance and Desorption Characteristics. *Ind. Eng. Chem. Res.* 2021, 60 (18), 6455–6464.
- [38] L.J. Lobree, A.W. Aylor, J.A. Reimer, A.T. Bell, NO Reduction by CH₄ in the Presence of O₂ over Pd-H-ZSM-5, *J. Catal.* 181 (1999) 189–204.
- [39] K. Chakarova, E. Ivanova, K. Hadjiivanov, D. Klissurski, H. Knözinger, Co-ordination chemistry of palladium cations in Pd-H-ZSM-5 as revealed by FTIR spectra of adsorbed and co-adsorbed probe molecules (CO and NO), *Phys. Chem. Chem. Phys.* 006 (2004) 3702–3709.
- [40] K. Hadjiivanov, J. Saussey, J.L. Freysz, J.C. Lavalley, FT-IR study of NO + O₂ co-adsorption on H-ZSM-5: Re-assignment of the 2133 cm⁻¹ band to NO⁺ species, *Catal. Letters.* 52 (1998) 103–108.
- [41] T. Salavati-fard, R.F. Lobo, L.C. Grabow, Linking low and high temperature NO oxidation mechanisms over Brønsted acidic chabazite to dynamic changes of the active site, *J. Catal.* 389 (2020) 195–206.
- [42] M. Che, J.F. Dutel, P. Gallezot, M. Primet, A study of the chemisorption of nitric oxide on PdY zeolite. Evidence for a room temperature oxidative dissolution of Pd crystallites, *J. Phys. Chem.* 80 (1976) 2371–2381.
- [43] M. Primet, Y. Ben Taarit, Infrared study of oxidized and reduced palladium loaded zeolites, *J. Phys. Chem.* 81 (1977) 1317–1324.
- [44] K. Mandal, Y. Gu, K.S. Westendorff, S. Li, J.A. Pihl, L.C. Grabow, W.S. Epling, C. Paolucci, Condition-Dependent Pd Speciation and NO Adsorption in Pd/Zeolites, *ACS Catal.* (2020) 12801–12818.
- [45] J. Lee, J. Kim, Y. Kim, S. Hwang, H. Lee, C.H. Kim, D.H. Kim, Improving NO_x storage and CO oxidation abilities of Pd/SSZ-13 by increasing its hydrophobicity, *Appl. Catal. B Environ.* 277 (2020) 119190.
- [46] R. Villamaina, U. Iacobone, I. Nova, E. Tronconi, M.P. Ruggeri, L. Mantarosie, J. Collier, D. Thompsett, Mechanistic insight in NO trapping on Pd/Chabazite systems for the low-temperature NO_x removal from Diesel exhausts, *Appl. Catal. B Environ.* 284 (2021) 119724.
- [47] K. Khivantsev, F. Gao, L. Kovarik, Y. Wang, J. Szanyi, Molecular Level Understanding of How Oxygen and Carbon Monoxide Improve NO_x Storage in Palladium/SSZ-13 Passive NO_x Adsorbers: The Role of NO⁺ and Pd(II)(CO)(NO) Species, *J. Phys. Chem. C.* 122 (2018) 10820–10827.
- [48] J. Xu, L. Ouyang, W. Mao, X.-J. Yang, X.-C. Xu, J.-J. Su, T.-Z. Zhuang, H. Li, Y.-F. Han, Operando and Kinetic Study of Low-Temperature, Lean-Burn Methane Combustion over a Pd/γ-Al₂O₃ Catalyst, *ACS Catal.* 2 (2012) 261–269.
- [49] G. Spezzati, Y. Su, J.P. Hofmann, A.D. Benavidez, A.T. DeLaRiva, J. McCabe, A.K. Datye, E.J.M. Hensen, Atomically Dispersed Pd–O Species on CeO₂ (111) as Highly Active Sites for Low-Temperature CO Oxidation, *ACS Catal.* 7 (2017) 6887–6891.
- [50] A. Bensalem, J.-C. Muller, D. Tessier, F. Bozon-Verduraz, Spectroscopic study of CO adsorption on palladium–ceria catalysts, *J. Chem. Soc., Faraday Trans.* 92 (1996) 3233–3237.
- [51] G.C. Cabilla, A.L. Bonivardi, M.A. Baltanás, Characterization by CO/FTIR spectroscopy

- of Pd/silica catalysts and its correlation with syn-gas conversion, *Catal. Letters*. 55 (1998) 147–156.
- [52] L. Castoldi, R. Matarrese, S. Morandi, P. Ticali, L. Lietti, Low-temperature Pd/FER NO_x adsorbers: Operando FT-IR spectroscopy and performance analysis, *Catal. Today*. 360 (2021) 317–325.